Supplementary Information

The supplement provides information on the time-frequency analysis as well as specifications on experimental setup of GENESIS 2.0.

Time-frequency analysis

Temporal changes in amplitude of signal components were estimated using a modified harmonic-filtering algorithm [1], which fits sinusoidal waves to a time series by means of least-squares. This method can process unevenly spaced time series directly, that is, without the requirement of prior interpolation. To obtain time-dependent amplitude estimates, the input time series is analyzed within a moving window of width $T_w = w \times T_f$, where $w = 3$ is a width–factor and T_f denotes the signal periodicity of interest (e.g. 20 ky). The window is shifted consecutively by one data point along the time axis of the input time series. Each "window segment" is linearly detrended prior to tapering with a Hanning window. The resulting amplitude and phase of the best-fit sinusoid are saved *vs.* the average of the observation times within the current segment and are used to reconstruct the signal component as function of time. The result of this procedure is equivalent to band-pass filtering [2]. The selected value of w offers a good compromise between statistical and systematic errors and results in a half-amplitude bandwidth of approximately $0.5/T_f$ cycles/My. Note that due to the finite window width, a step-like increase in signal amplitude appears $w \times T_f$ wide. Applying the above filtering algorithm over a predefined range of frequencies allows us to detect changes in signal components in time-frequency space [3]. The dependence of window width, T_w on frequency leads to a change in temporal resolution with frequency. At low (high) frequencies wide (narrow) windows result in a low (high) temporal resolution. This scale dependence of the

temporal resolution is similar to that of wavelet analysis. A program for time-frequency analysis (TIMEFRQ, version 4.3) is available from www.palmod.uni-bremen.de/~mschulz. In the following we apply the algorithm to the time and to the depth domain. To avoid double meaning, we refer to the method in both cases as time-frequency analysis.

Time-series analysis of nannofossil zone CC15 and the upper part of the profile.

To detect persistent periodicities in the geochemical records we conducted time-frequency analysis using TOC and K/Al records from ODP Site 959 using the above method. Initially, analyses were performed in the depth domain in the intervals 1041.81 – 1028.62 mbsf (CC15, Figure S1 A and B) and 1022.69 – 1005.43 mbsf (CC16, Figure S1 C and D). The time-frequency analysis in CC15 reveal only one prominent frequency of more than 3 cycles/m at the base that shifts to about 1.3 cycles/m above 1037 mbsf. No persistent signal components are detected at shorter wavelength. The low-frequency signal near 0.7 cyles/m recognized between ~1035 and 1036 m for TOC (Fig S1 B) is an artefact, reflecting the interruption of the typical TOC cycle pattern in that interval. The upper part of profile between 1022.69 – 1005.43 mbsf (Figure S1 C and D) also shows one prominent frequency at about 1.8 cycles/m that progressively decreases upward to about 1.3 cycles/m. This dominant frequency disappears between 1016 and 1012 mbsf due to the strong attenuation of amplitudes in that part of the section (see records in Figs S1 C and D). These results support the notion that only one dominant cycle persists throughout the record and that the frequency of this cycle varies only slightly from ~1037 mbsf upward. Minor variations in sedimentation rate across the section likely explain small modulations in the prominent m-scale frequency.

In a second step, we attempted to estimate the period of the dominant cycle in the time domain, by analyzing the data from nannofossil biozone CC15 above 1041 mbsf in a chronostratigraphic framework. This approach bears some uncertainties and limitations that have to be addressed prior to the presentation of the results from time-frequency analysis. A high-quality age model is pivotal for any precise identification of periodic signal components. This requirement poses a fundamental problem for any Cretaceous high-resolution record. Providing such a high-quality age model for Site 959 that resolves with sufficient reliability orbital-scale variability has been shown to be critical if not impossible. This is primarily due to poor preservation of calcareous tests from foraminifera and coccoliths [4,5] but also because of deposition of the sediments during Magnetochron C34n (121-83 Ma), the "Cretaceous Quiet Zone" [6]. Watkins et al. (1998) [5] describe non-calcareous claystone between 1027 – 870 mbsf, excluding any biostratigraphic time control in the upper part of the study section. Below 1027 mbsf, nannofossil assemblages are sparse but fortunately sufficient to allow the assignment of nannofossil biozones CC16 to CC14 [5].

The central part of the OAE 3 at Site 959 thus reveals two reasonably well located biostratigraphic age fixpoints, i.e. the first occurrence of *Reinhardtites anthophorus* (boundary CC14/CC15) and the first occurrence of *Lucianorhabdus cayeuxii* (boundary CC15/CC16). The uncertainty in boundary location for both fixpoints range from 56 cm at CC14/CC15 to 84 cm at CC15/CC16 [5]; the total length of CC15 in the core may thus vary between 14 m and 12.6 m, the uncertainty being equivalent to about two geochemical cycles. Both datum events also vary in absolute age depending of the chronostratigraphy applied. Gradstein et al. (1995) [7] give ages of 85.66 and 84.9 Ma for the boundaries of CC14/CC15 and CC15/CC16, respectively. In a more recent

chronostratigraphy, numerical ages of 85.5 and 84.8 Ma are given for both datum events [8]. The total age uncertainty for CC15 is therefore about 0.1 Ma, without consideration of any error of these datums. Finally, sedimentological evidence strongly supports that sedimentation rates at Site 959 have not been constant across the study interval. Hardgrounds, reworked debris, and condensed sections indicate strongly reduced sedimentation rates below about 1040.5 mbsf (about 2.5 m/Ma [5,6]). In the middle and upper part of CC15 sedimentation rates increase by one order of magnitude to values of 20-40 m/Ma [9] consistent with a palaeobathymetric position at upper continental margin at that time [10]; linear interpolation of absolute age between the aforementioned age fixpoints of biozone CC15 must therefore result in an erroneous age model if the drastic change in sedimentation rate is not taken into account. We conclude that uncertainties in the duration of nannofossil biozone CC15, the location of boundaries of biozone CC15 at Site 959, and drastic changes in sedimentation rate in the lower part of the section at Site 959 are significantly variable; a fact that allows for a rather large inaccuracy of statistically-deduced time frequencies.

To minimize at least the uncertainty due to drastic changes in sedimentation rate for time-series analysis we omitted data below 1041.17 mbsf, i.e. the lowermost two cycles in CC15 that were before tentatively assigned to 100 ka eccentricity cycles [11]. Using the chronostratigraphy from ODP Leg 207 [8], we linearily interpolated ages between 1041.17 mbsf (85.3 Ma, subtracting 200 ka for the two omitted 100 ka cycles) and 1028.62 mbsf (84.8 Ma, top of CC15). The time-frequency analysis for TOC and K/Al display one prominent frequency at about 35 cycles/Ma throughout main parts of the record (Figure S1 E and F). Based on the age model, this frequency corresponds to a period of about 28 ka. Considering the potential uncertainties of the age model, this

period lies in the range of orbital frequencies and close enough to 22 ka to support precession as the prominent frequency. Considering the outlined uncertainties at Site 959 we consider this conclusion as robust as possible and difficult to improve.

Time-frequency analysis does not identify other significant frequencies that persist across the record. The only hint comes from the records of mean square values of K/Al and Ti/Al that may suggest a 400 ka frequency. A 100 ka and/or 41 ka component is not identified in the time-series analysis. This result may come as a surprise given the high time-resolution and continuity of the records. One argument to explain this observation may be the location of the study area a few degrees south of the palaeo-equator. At this latitude it appears reasonable to expect a prominent precessional signal (even doubling of the precessional frequency). However, we do not have a conclusive physical explanation for the absence of the 100 ka and 41 ka signals.

References for first part of the supplement

1. Ferraz-Mello, S. Estimation of periods from unequally spaced observations. *Astronom. J.* **86,** 619-624 (1981).

2. Hinnov, L.A., Schulz, M. & Yiou, P. Interhemispheric space-time attributes of the Dansgaard-Oeschger oscillations between 100 and 0 ka. *Quat. Sci. Rev.* **21,** 1213-1228 (2002).

3. Schulz, M., Berger, W.H., Sarnthein, M. & Grootes, P.M. Amplitude variations of 1470-year climate oscillations during the last 100,000 years linked to fluctuations of continental ice mass. *Geophys. Res. Lett.* **26,** 3385-3388 (1999).

4. Bellier, J.P. Cretaceous planktonic foraminifers, eastern Equatorial Atlantic. *ODP Sci.Res.* **159,** 335-345 (1998).

5. Watkins, D.K., Shafik, S. & Shin, I.C. Calcareous nannofossils from the Cretaceous of the Deep Ivorian Basin. *ODP Sci.Res.* **159,** 319-333 (1998).

6. Pletsch, T. *et al.* Cretaceous separation of Africa and South America: the view from the West African margin (ODP Leg 159). *J. of South Am. Earth Sci* **14,** 147-174 (2001).

7. Gradstein, F.M. *et al.* in *Geochronology, Time Scales and Global Stratigraphic Correlation* (eds Berggren, W.A., Kent, D.V., Aubra, M.P. & Hardenbol, J.) 95-126 (Spec. Publ. 54, SEPM, Washington, 1995).

8. Shipboard Scientific Party. Explanatory notes. *In* Erbacher, J., Mosher, D.C., Malone, M.J., et al., *Proc. ODP, Init. Repts.* 207, 1-94 [CD-ROM] (2004). Available from: Ocean Drilling Program, Texas A&M University, College Station TX 77845-9547, USA.

9. Wagner, T., Sinninghe Damsté, J.S., Hofmann, P. & Beckmann, B. Euxinia and primary production in Late Cretaceous eastern equatorial Atlantic surface waters fostered orbitally driven formation of marine black shales. *Paleoceanography* **19,** doi:10.1029/2003PA000898 (2004).

10. Holbourn, A.E.L. *et al.* in *The Oil and Gas Habitats of the South Atlantic* (eds Cameron, N.R., Bate, R.H. & Clure, V.S.) 195-222 (Spec. Publ. 153, Geol. Soc., London, 1999).

11. Hofmann, P., Wagner, T. & Beckmann, B. Millennial- to centennial-scale record of African climate variability and organic carbon accumulation in the Coniacian-Santonian eastern tropical Atlantic (Ocean Drilling Program Site 959, off Ivory Coast and Ghana). *Geology* **31,** 135-138 (2003).

Supporting Online Figure S1: Time-frequency analysis of K/Al and TOC records from ODP Site 959. Analysis were performed in the depth domain separately for the lower (A, B) and upper (C, D) parts of the record. Time-domain analysis was only carried out for the older part of the series (E, F). Bottom panel in each graph shows the record being analysed (K/Al and TOC in [wt. %]), while top panel shows signal amplitudes (in the same units as the data being analyzed) as function of depth/time and frequency.

A – ODP 959, K/Al (CC15) versus depth

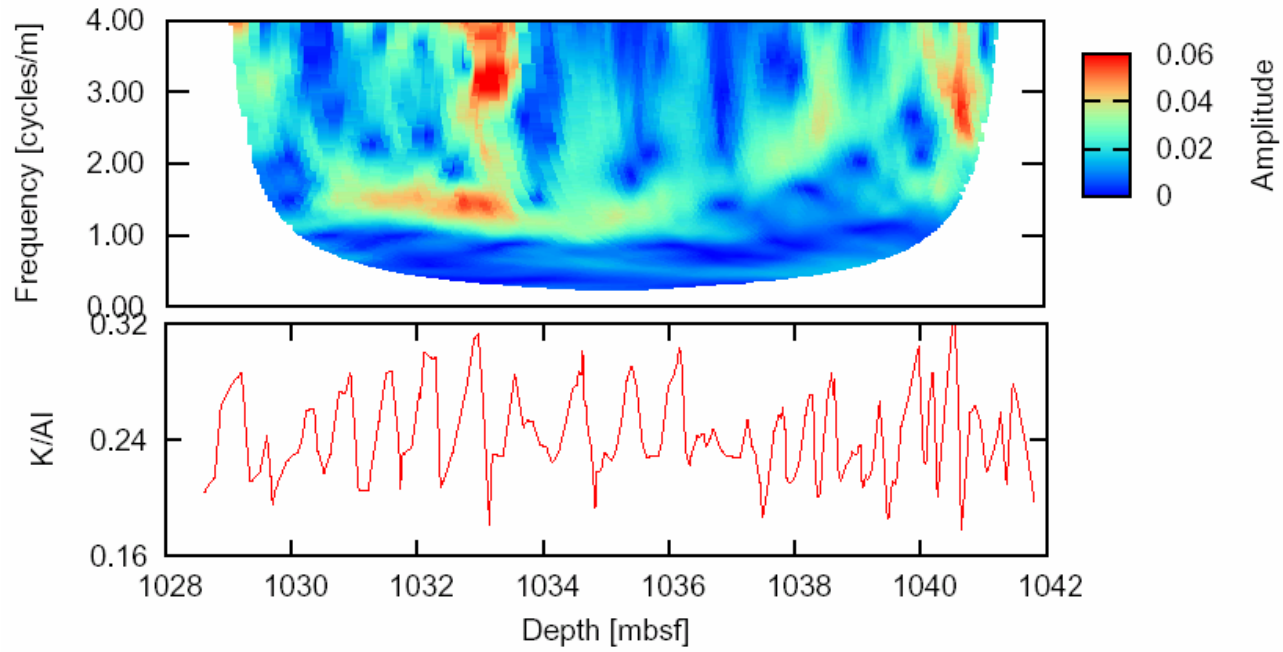

B – ODP 959, TOC (CC15) versus depth

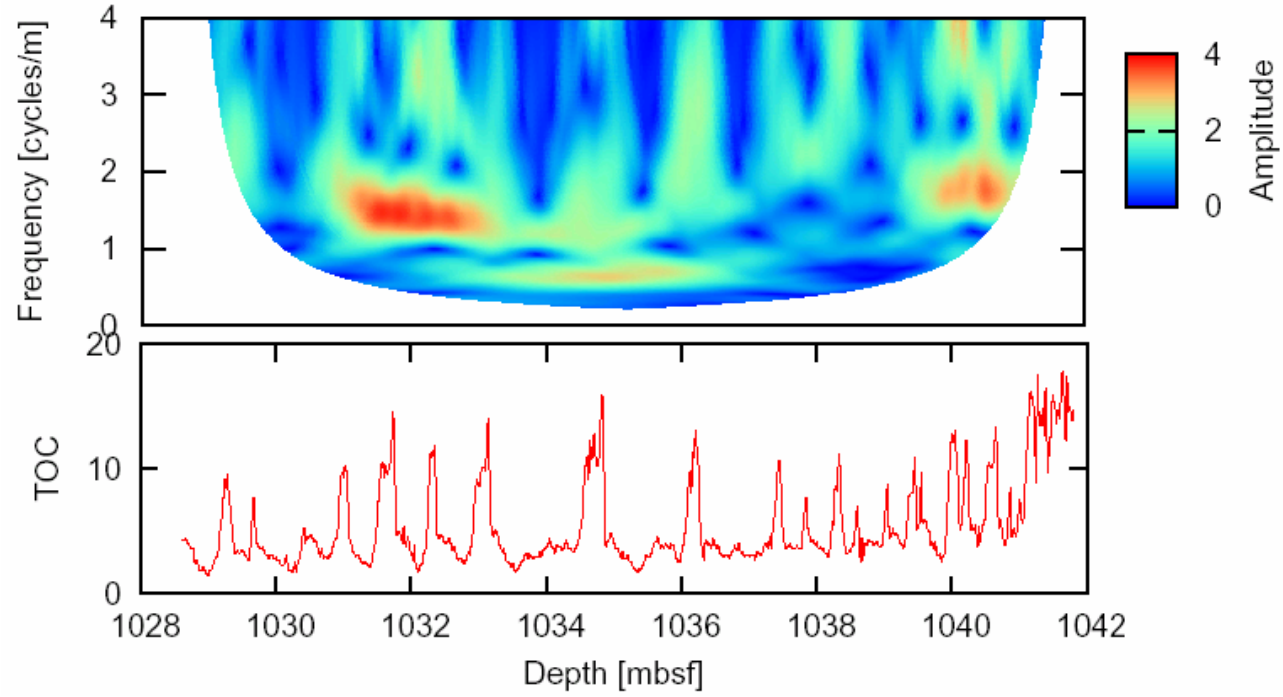

C – ODP 959, K/Al versus depth

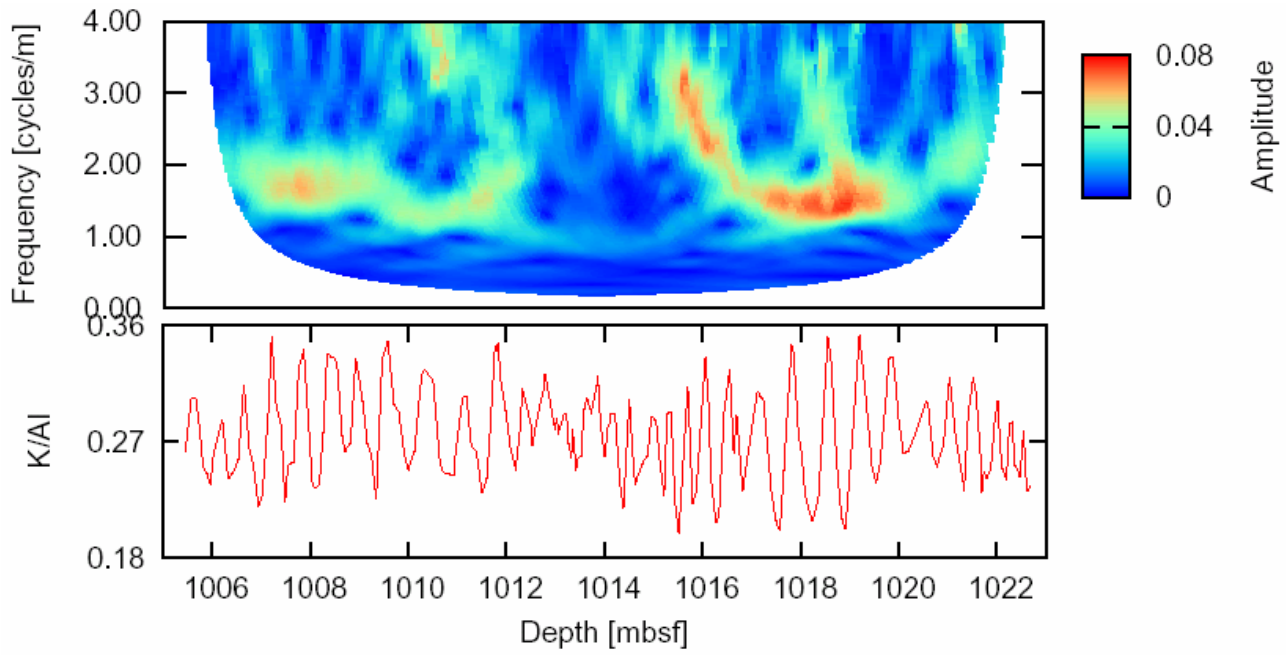

D – ODP 959, TOC versus depth

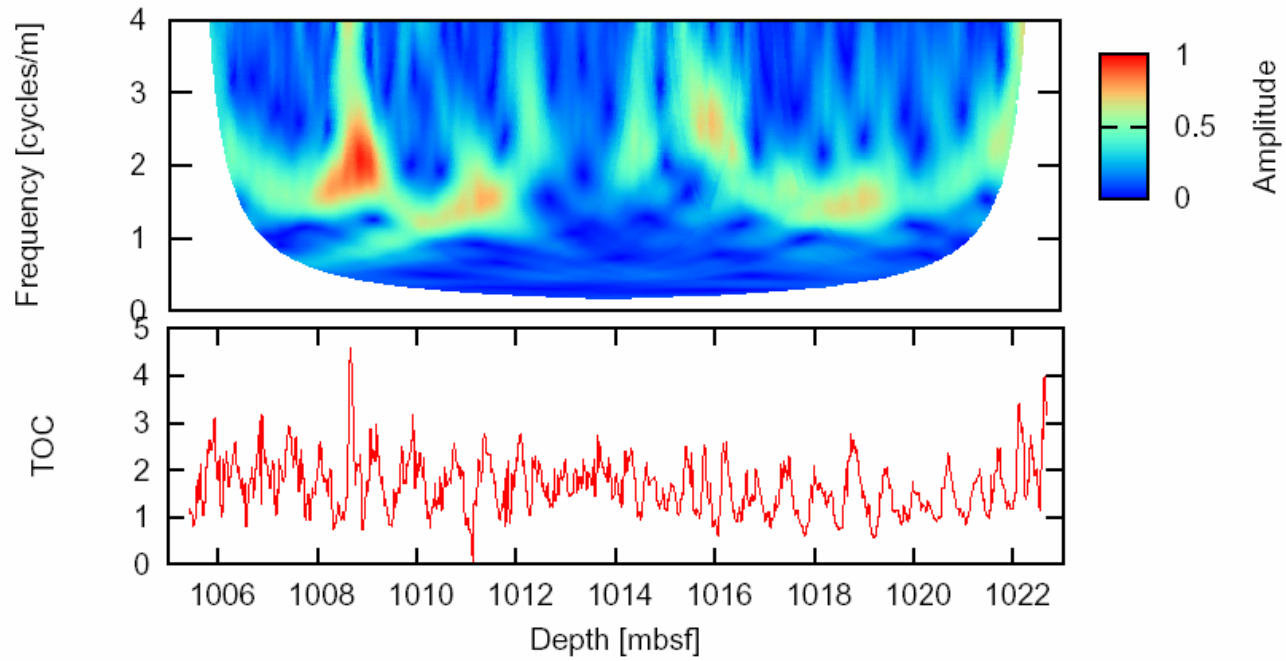

Supporting Online Figure S1: continued.

E – ODP 959, K/Al versus age

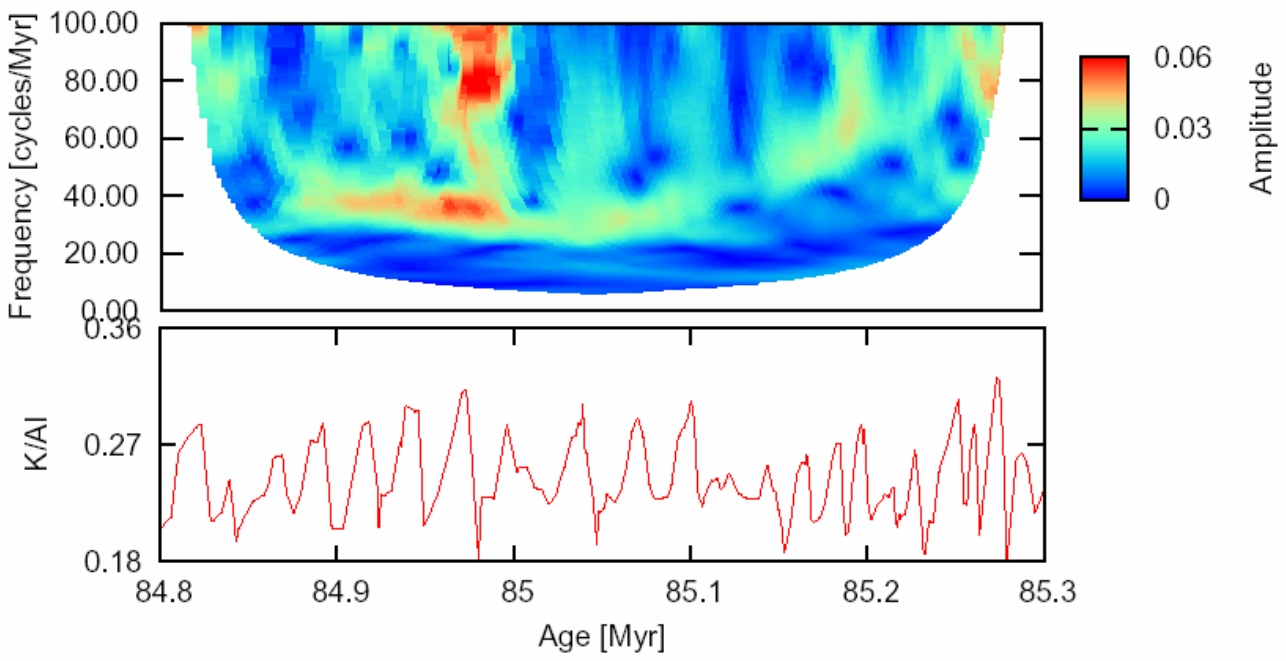

F – ODP 959, TOC versus age

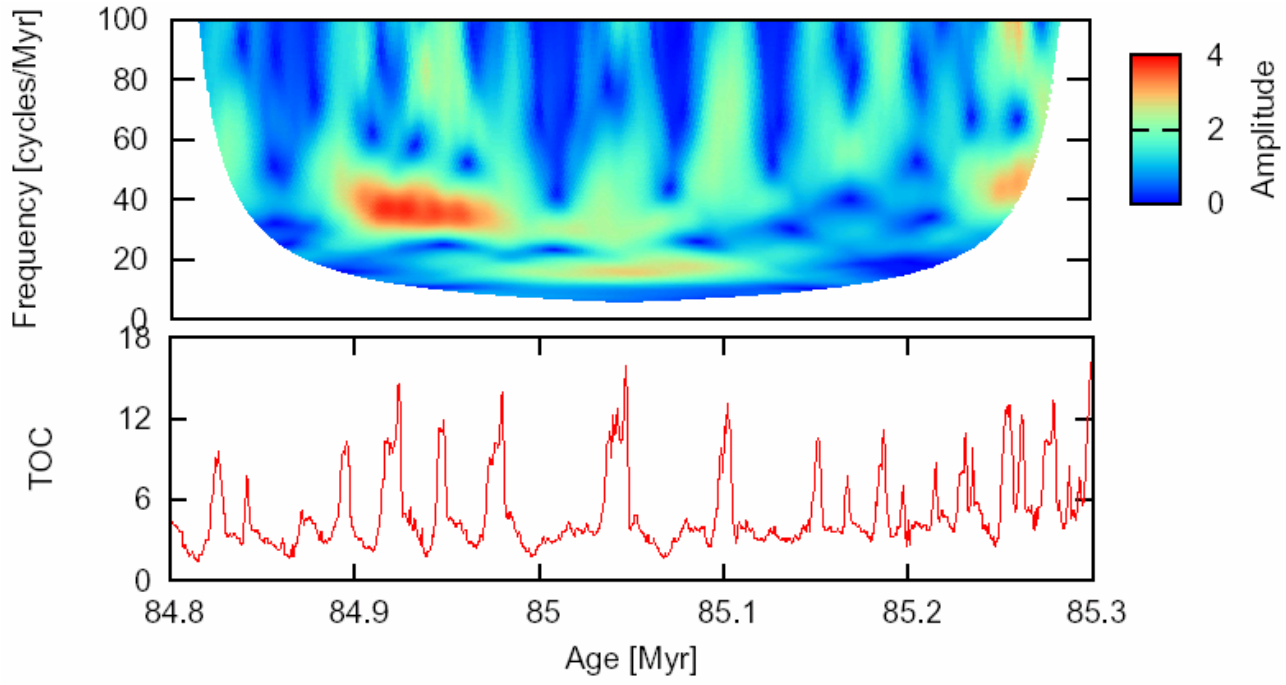

Supporting Online Figure S1: continued.

The second part of the supplement provides specifications on experimental setup of GENESIS 2.0, paleogeography, astronomical forcing, and significance and effectiveness including sensitivity tests and other critical aspects to model sensitivity and validation of the simulated data.

Global circulation model GENESIS 2.0 and experimental setup. GENESIS v. 2.0 consists of an atmosphere general circulation model coupled to a non-dynamic 50-m slab ocean model. The atmospheric component has 18 vertical layers with a spectral resolution of T31, corresponding to a Gaussian latitude-longitude grid of 3.758° x 3.758°. Coupled to the atmospheric models are surface models having a 2° x 2° resolution: sea-ice, snow, vegetation and a six-layer model of soil. Boundary conditions set for Cenomanian-Turonian simulations are as follows: The solar constant was specified to be 98.62 % (1337.0 W/m^2) of the present value of 1365.0 W/m^2 based on estimates of solar luminosity. Heat transport in the slab ocean model was prescribed with values similar to those of today. Atmospheric CO_2 was specified as 1881.6 ppm, about five times the 2003 average value of 376.3 ppm. Recent re-evaluation of CO_2-values has shown that Upper Cretaceous values have been in the range between 1.5 and 7 times "present", with 5x being the best estimate [1]. Concentrations of atmospheric CH_4 and N_2O were set at pre-industrial levels, 0.800 ppm and 0.288 ppm, respectively. A single vegetation, "Type 6" (broadleaf trees with groundcover – savannah) [2] was specified and assumed to cover all land areas. The soil was specified as consisting of 51% sand, 29% silt, and 20% clay, distributed uniformly over all land areas. The model was allowed to spin up for 25 years, datasets were then compiled by averaging years 15 through 25.

Paleogeography. The paleogeographic boundary conditions (land-sea distribution) were provided by a global paleogeographic reconstruction for the early Turonian prepared for these simulations [3]. This map was constructed using the techniques

involved in producing the Paleozoic and Mesozoic-Cenozoic Atlases of "Lithological-Paleogeographic Maps of the World" [4]. The original data, from which the maps are constructed, taken from the literature and other sources, are originally plotted on large-scale equal area maps of each continent. The lithologic information is interpreted in the context of the paleogeographical environments and tectonic regimes which governed erosion and sediment deposition. The data are then smoothed and transferred onto a smaller scale global present day map. Elevations are originally estimated qualitatively based on the masses and grain size of the detrital sediment eroded and deposited in adjacent basins. The quantitative topographic interpretation is based on an interpretation of the denudation rate over the eroded region calculated from the volume of sediment supplied to the adjacent basins, using an estimate of the erosion-rate/elevation relationship. The map shows continents in their present-day configurations. It was digitized and the appropriate areas assigned to the continental blocks and terranes. Using a plate tectonic reconstruction program (www.odsn.de), these fragments were rotated back to their Turonian (93 Ma) position. The paleogeography, terrestrial elevations, and vegetation of this plate tectonic map were then converted to the 2° x 2° resolution of the surface model used to define paleo-shorelines and land-surface boundary conditions.

Astronomical Forcing. Five simulations with changing orbital forcing were carried out. For the control run, we assume that the Earth's orbit around the Sun was circular (eccentricity = 0) and had an obliquity of 23.5°. The remaining four simulations were computed with different positions of the earth in the precession cycle (0 = spring, 90 = winter, 180 = autumn, and 270 = summer). The so-called "climatic precession" determines which season coincides with perihelion (Earth's smallest distance to the sun). This allows analysis of the changes during one complete precessional cycle, including both of the solstice end members and the two equinoctial passages. Eccentricity for these runs was fixed at a value of 0.05. Obliquity was fixed at the

present value of 23.5°. By definition the origin (0°) and end (360°) of the precession cycle are set at the northern hemisphere vernal equinox.

Model sensitivity and validation. Global paleoclimate modes such as GENESIS 2.0 are not specifically designed to simulate regional precipitation and discharge patterns, and seasonality for small geographic areas with large precision. We therefore conducted sensitivity tests and considered various other critical aspects to validate the quality of the simulated data.

The sensitivity experiments addressed surface runoff, drainage, continental discharge, and wind velocities. First we compare simulated precipitation data from GENESIS for modern NW-Africa (9-19°N / 9°W-9°E) to measured and modelled data from the literature. Modern annual precipitation for the region of 10-20°N / 10°W-10°E is measured to be 638 mm/year [5]. GENESIS 2.0 provides modern annual precipitation values of 642 mm/day at 2 m height above surface (D. Pollard, Pennsylvania State University, unpublished data), which are above the 95% confidence level of the predicted values provided by satellite measurements (*http://www.cpc.ncep.noaa.gov/products/african_desk/meteosat/*) testifying to the quality and significance of GENESIS 2.0-derived modelling data

Recent advances focus on the implementation of an explicit river routing scheme for the use in paleoclimate GCM [6]. An explicit river routing scheme is currently developed for a future version of GENESIS but is not available yet. We want to emphasize that application of river routing scheme, although desirable, is not necessary for the central aims and interpretations of our study. This is because our conclusions base on estimates of total continental freshwater discharge that flows into the mid-Cretaceous Deep Ivorian Basin. It is not critical to specifically know where the local total continental freshwater discharge in the chosen rectangle (25-55°W, 1-17°S) emerged on the Mid-Cretaceous African coast. From previous studies [7-9] we know that we would get similar

results as described in our study because precipitation and discharge patterns in GENESIS do not vary considerably over small scales.

The application of a river routing treatment would delay the seasonal peak of discharge by several weeks, at least while the fresh water is en route towards the coast. For the modern Amazon basin, for example, the delay may actually be up to several months (peak precipitation in January - peak river discharge in May) [10]. Since the Mid-Cretaceous river system in low-latitude N-Africa may be assumed to be considerably shorter than the present day Amazon one, it appears reasonable to expect a delay time on the order of a few weeks. The point we want to make is that this time delay has *no impact* on the principle conclusions drawn from our modeling results. Instead, it is the amplitude of peak continental freshwater discharge for the four orbital cases that is critical for understanding Upper Cretaceous black shale formation.

We finally considered the question of alternative hypotheses/processes, such as upwelling. The geochemical records from ODP Site 959 do not support such a mechanism. Instead they show that periods of organic carbon burial follow humid time intervals with indication for high continental discharge and not intervals with enhanced wind strength [11-13]. This interpretation is also supported by supplementary results from modelling (S. Flögel, IFM-GEOMAR, unpublished results). We analyzed global and regional pressure systems and wind velocities, focusing on the study area. The results from wind field patterns for all five models suggest that upwelling was not likely to have occurred in the Deep Ivory Basin. Only southerly sideshore winds blowing parallel to the coastline would be able to invoke Ekman transport of surface water away from the continent, therefore enabling upwelling. Offshore winds in addition could invoke coastal upwelling. No offshore or sideshore winds have been simulated for the coastal areas of the Deep Ivorian Basin using AGCM. Based on these independent and

consistent results from geochemical data and simulations we did not put effort in running an additional ocean model.

References for second part of the supplement

1. Royer D.L., Berner, R.A., Montanez, I.P., Tabor, N.J., & Beerling, D.J. CO_2 as a primary driver of Phanerozoic climate. *GSA Today* **14**, no. 3, 4-10 (2004).

2. Dorman, J.L. & Sellers, P.J. A global climatology of albedo, roughness, length and stomatal resistance for atmospheric general circulation models as represented by the simple biosphere model (SiB). *American Meteorological Society* **28**, 833-855 (1989).

3. Balukhovsky, A.N., Floegel, S., Hay, W.W., Migdisov, A., & Wold, C.N. A paleogeographic map for the Lower Turonian. *EarthRef Digital Archive* http://earthref.org/cgi-bin/erda.cgi?n=220 (2004).

4. Ronov, A. B., Khain, V., & Balukhovsky, A. *Atlas of Lithological-Paleogeographical Maps of the World, Mesozoic and Cenozoic of Continents and Oceans* (eds. Barsukov, V. & Laviorov, N.) 79 pp. (U.S.S.R. Academy of Sciences, Leningrad, 1989).

5. T.A. Shver & L.R. Struzer in *World water balance and water resources of the Earth* (eds Korzun, V.I., Sokolov, A.A., Budyko, M.I., Voskresensky, K.P., Kalinin, G.P., Konoplyantsev, A.A., Korotkevich, E.S., Kuzin, P.S., and Lvovich, M.I.) 256-265 (Studies and Reports in Hydrology 25, 1978).

6. Markwick, P. J. & Valdes, P. J. Palaeo-digital elevation models for use as boundary conditions in coupled ocean–atmosphere GCM experiments: a Maastrichtian (late Cretaceous) example. *Palaeogeogr., Palaeoclimatol., Palaeoecol.* **213**, 37-63 (2004).

7. Poulsen, C.J., E.J. Barron, C.C. Johnson & P.J. Fawcett in *The Evolution of the Cretaceous Ocean-Climate System* (eds Barrera, E. & Johnson, C.) 73-90 (Spec. Pap. 332, Geol. Soc. of Am., Boulder, 1999).

8. Floegel, S., Hay W.W., DeConto, R.M., & Balukhovsky, A.N. Formation of sedimentary bedding couplets in The Western Interior Seaway of North America -

Implications from Climate System Modeling. *Palaeogeogr., Palaeoclimatol., Palaeoecol.* **218,** 125-143 (2005).

9. Flögel, S. On the Influence of Precessional Milankovitch Cycles on the Late Cretaceous Climate System: Comparison of GCM-Results, Geochemical, and Sedimentary Proxies for the Western Interior Seaway of North America. *Doctoral Thesis, University of Kiel, Germany*, 236 pp., Electronical dissertation: http://e-diss.uni-kiel.de/diss_552/, pp. 231 (2002).

10. Marengo, J.A., Miller, J.R., Russell G.L., Rosenzweig C.E., & Abramopoulos, F. Calculations of river-runoff in the GISS GCM: Impact of a new land-surface parameterization and runoff routing model on the hydrology of the Amazon River. *Climate Dynamics* **10**, 349-361 (1994).

11. Hofmann, P., Wagner, T. & Beckmann, B. Millennial- to centennial-scale record of African climate variability and organic carbon accumulation in the Coniacian-Santonian eastern tropical Atlantic (Ocean Drilling Program Site 959, off Ivory Coast and Ghana). *Geology* **31,** 135-138 (2003).

12. Beckmann, B., Wagner, T. & Hofmann, P. in *The deposition of Organic Carbon-Rich Sediments: Models, Mechanisms, and Consequences* (Ed. Harris, N.B.) 125-143 (Spec. Pub. 82, SEPM, Washington, 2005).

13. Wagner, T., Sinninghe Damsté, J.S., Hofmann, P. & Beckmann, B. Euxinia and primary production in Late Cretaceous eastern equatorial Atlantic surface waters fostered orbitally driven formation of marine black shales. *Paleoceanography* **19,** doi:10.1029/2003PA000898 (2004).